Multiscale analysis of urban thermal characteristics: case study of Shijiazhuang, China

Kai Liu
Xiaohong Zhang
Xueke Li
Hailing Jiang

SPIE

Multiscale analysis of urban thermal characteristics: case study of Shijiazhuang, China

Kai Liu,[a,b] Xiaohong Zhang,[a,*] Xueke Li,[a,b] and Hailing Jiang[a,c]
[a]Chinese Academy of Sciences, Institute of Remote Sensing and Digital Earth,
The State Key Laboratory of Remote Sensing Sciences, Beijing 100101, China
[b]Graduate University of Chinese Academy of Sciences, Beijing 100049, China
[c]Peking University, Institute of Remote Sensing and GIS, Beijing 100871, China

Abstract. The urban heat island (UHI) effect caused by urbanization generally leads to adverse economic and environmental impacts. Thus, a detailed assessment of the thermal properties over individual land cover types at different spatial resolutions is required to better understand the establishment of UHI. Two scale levels are utilized to examine surface thermal characteristics in the case of Shijiazhuang, China. At the regional level, Landsat TM data are used to extract sub-pixel impervious surface area (ISA) and to inverse land surface temperature (LST) by means of multiple endmember spectral mixture analysis. Urban thermal characteristics are analyzed by relating the LST to normalized difference vegetation index (NDVI) and ISA. On the other hand, thermal airborne spectrographic imager data, with a high spatial resolution, are employed to describe the spatial distribution of urban thermal patterns at the local level. Results indicate that there is an approximate linear relationship among LST, NDVI, and ISA. In addition, the thermal characteristics over each land cover type are consistent at both levels, suggesting UHI is evident at Shijiazhuang and impervious surface is contributing most to this phenomenon. This confirms that different spatial scales are requested in UHI studies. © *2014 Society of Photo-Optical Instrumentation Engineers (SPIE)* [DOI: 10.1117/1.JRS.8.083649]

1 Introduction

Land surface temperature (LST) is vital in understanding biodiversity and surface energy balance, as well as climatological changes.[1,2] One of the climate phenomena associated with LST is urban heat island (UHI), which leads to a higher temperature in urban areas than surrounding areas. Recently, more and more studies of UHI are based on remote sensing, in which surface temperature is retrieved to demonstrate its relationship with other biophysical processes. Moderate-resolution imaging spectroradiometer and advanced very-high-resolution radiometer data are initially utilized to derive LST and examine the temporal and spatial pattern of surface temperature. However, these data with large spatial resolution are unsuitable for exploring accurate and meaningful relationships among LST and surface cover characteristics.[3–6] Later, the availability of LST through LANDSAT and advanced spaceborne thermal emission and reflection radiometer (ASTER) with a medium spatial resolution has significantly facilitated studying temperature variations.[7–9] Additionally, airborne thermal data are proven to be an alternative means to investigate the UHI phenomena due to their high performance in inverting actual LST.[10–13]

Vegetation and urban impervious surface are two vital components in the studies of UHI. Vegetation can mitigate the influence of UHI by controlling the surface temperature in the process of surface energy balance. Numerous studies have been devoted to studying the

coherence of LST and the normalized difference vegetation index (NDVI), revealing a strong negative correlation among them.[14–16] Impervious surfaces, a type of manmade land-cover type through which water cannot infiltrate into soil, are primarily present in cities with the forms of transportation and building rooftops.[17] The increasing impervious surface is relative to urbanization expansion, and generally goes along with the change in surface heat flux contributing to the UHI. Thus, analysis of the relationship between LST and percent impervious surface area (% ISA) in an urban area provides an alternative method for the research of UHI phenomena.[18–20] Linear spectral mixture analysis (LSMA) is a quite commonly used technique for extracting impervious surfaces and deriving surface temperature because of its effectiveness in handling the pixel mixture problem. Through quantifying and mapping an urbanized environment with vegetation-impervious surface-soil (VIS) model, LSMA is superior to traditional land classification in preserving the heterogeneity of urban cover, especially for medium-resolution imagery.[21,22] The multiple endmember spectral mixture analysis (MESMA) method[23,24] is found to be better than other spectral mixture methods, as its estimation error is relatively smaller. However, far fewer studies have been dedicated to investigating the imperviousness and surface thermal response by means of MESMA.

In this paper, a methodology combing MESMA with NDVI thresholds method is proposed to retrieve LST from Landsat imagery. Qualitative and quantitative analyses, which focus on regional level with Landsat TM and local level with airborne hyperspectral thermal data, have also been carried out to determine urban surface thermal patterns. The primary objectives of this research are to (1) extract subpixel ISA through MESMA and further verify its precision with actual proportion values; (2) retrieve surface temperature from the Landsat TM thermal band using spectral mixture method; (3) analyze the urban thermal characteristics by extensively studying the relationships among LST, ISA, and NDVI; and (4) describe the spatial distribution of urban thermal patterns with airborne thermal imagery.

2 Study Area and Data

2.1 Study Area

The city of Shijiazhuang (Lat. 38°03′N, Lon. 114°29′E) is located in north China (Fig. 1), with an area of ∼658 square kilometers. It spreads across two geomorphic units in the Taihang Mountains and the North China Plain. Situated at the eastern edge of the Eurasian plate and close to the Pacific Ocean, Shijiazhuang belongs to the warm temperate continental monsoon climate.

With a current population of ∼5 million, Shijiazhuang is the capital of the Hebei Province and is important as the major center of culture, industry, commerce, and transportation. Moreover, Shijiazhuang is a significant region where UHI has played an important role in influencing local energy consumption and climatological variation. Investigating and analyzing the urban thermal landscape is meaningful for controlling and planning the city's future development. Thus, as one of the largest cities in north China, Shijiazhuang is selected to explore the relationship among LST and other surface characteristics.

2.2 Remote Sensing Data and Field Data Acquisition

A Landsat TM image of June 28, 2010 (acquisition time: approximately 10:51 a.m.), was selected on account of its availability and good quality. TM image was geo-referenced to the Universal Transverse Mercator coordinate system based on the high-resolution Google Earth™ imagery and WorldView-2 (WV2) imagery, with a root mean square error (RMSE) of rectification <0.5 pixels. The thermal airborne spectrographic imager (TASI) data used in this study were collected at an altitude of 1 km, from 10:30 to 11:00 local time on August 15, 2010. Table 1 indicates the characteristics of TASI sensor. The coverage area of this airborne thermal imagery is the center of Shijiazhuang, with a total area of ∼40 square kilometers. A field campaign was conducted in step with the airborne flight. The actual LST of some selected natural and artificial surface features was measured in 10 min before or after the overpass of the flight,
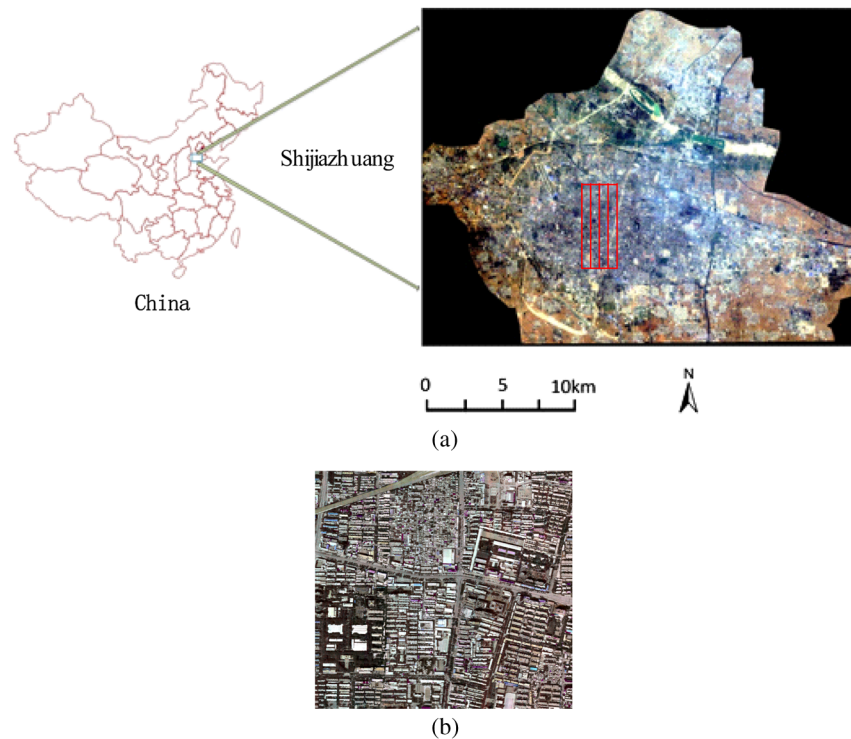
(a)

(b)

Fig. 1 Study area in Shijiazhuang, China. (a) Location of the study area and LANDSAT 5 TM imagery. (b) Partial TASI-600 RGB false-color composite of the study area ($R = 11.5$ μm, $G = 10.35$ μm, and $B = 9.149$ μm).

Table 1 Thermal airborne spectrographic imager (TASI) sensor characteristics.

Parameter	Value
Spectral range (μm)	8 to 11.5
Spectral width (μm)	0.1095
Number of bands	32
Instantaneous field of view	0.068 deg
Field of view	40 deg
Across track pixels no.	600
Signal quantization level	14 bits

using thermal infrared spectrum radiometer (CE312). Meanwhile, an analytical spectral device spectroradiometer (covering the spectrum of 0.35 to 2.5 μm) as well as SVC HR-1024 field spectroradiometer (Spectra Vista Corporation, Poughkeepsie, NY; covering the spectrum of 0.35 to 2.5 μm) was used to collect their spectral signatures during July 25 to August 20, 2010. The broadband spectral emissivity data of these objects were concurrently collected with portable emissivity measurement instruments.

In addition, a scene of WV2 imagery of September 15, 2010, was purchased for this study. It contains one panchromatic band and four multispectral bands, the spatial resolutions of which are 0.5 and 2 m, respectively. Short-wave and near-infrared imagery (covering the spectrum of 0.9 to 2.5 μm) was acquired by short-wave-infrared airborne spectrographic imager (SASI) sensor on August 15, 2010. This image would be merged with the WV2 image to perform assessment in terms of a classification map.
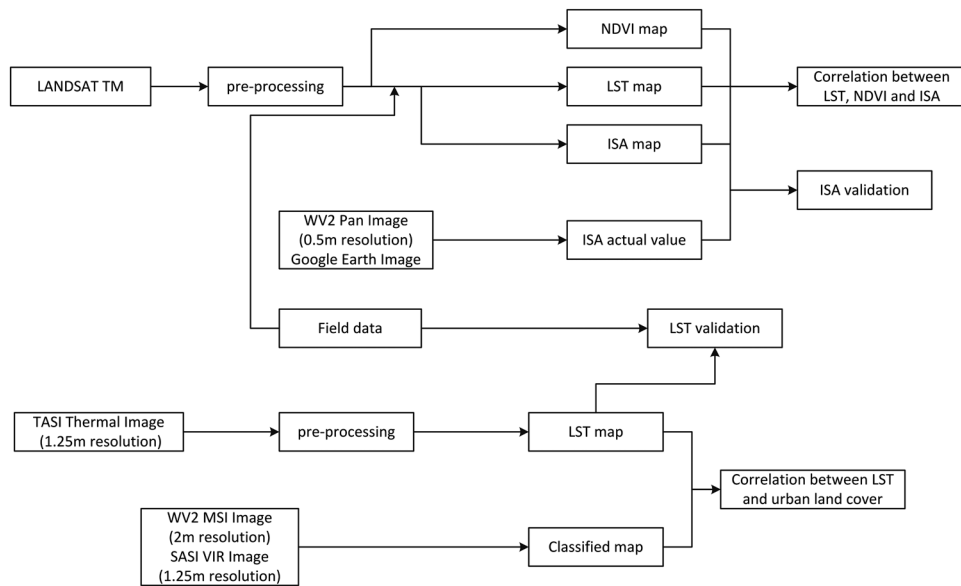
Fig. 2 Overall process flow.

3 Methodology

As previously mentioned, this study was conducted at two different scales: medium spatial resolution with Landsat sensor and high spatial resolution with TASI sensor. The overall processing scheme of this research is displayed in Fig. 2.

3.1 *Image Preprocessing*

The raw values of Landsat TM 1 to 5 and 7 bands were first converted to at-satellite radiance and then converted to at-satellite reflectance and surface reflectance. Atmospheric correction was applied to this image using the fast line-of-sight atmospheric analysis of spectral hypercubes module in ENVI 4.8. Additionally, based on the surface reflectance, NDVI was computed to help us understand the relationship between LST and urban vegetation fractions.

According to the assumption that the radiometric response of spectral emissive detector is linear, TASI imagery was calibrated pixel by pixel with the gain and offset of the response function. Atmospheric correction was applied to this airborne thermal image. The parameters required in this process were acquired by a common radiative transfer code, MODTRAN.

3.2 *Methodology of Impervious Surface Fractions Retrieval*

MESMA was implemented to retrieve impervious surface fractions using Landsat imagery. This method allows for the variation in both type and number of endmembers inside a pixel, resolving the problem of spatial heterogeneity and spectral variability.[25] It mainly contains two steps: spectral library construction and spectral unmixing analysis.

Developing a spectral library is critical for MESMA, in which V-I-S model is adopted to select major spectral characteristics. In our research, shade was included as an additional spectral since it commonly exists in most urban areas. The shade spectral was realized to be 1% in all bands. Endmember spectra involving impervious surface, bare soil, and vegetation were identified from field acquisition and image itself. Additionally, water area was extracted and masked in the preprocessing using automated water extraction index.[26]

Varieties of field spectra were acquired using a spectral acquisition instrument from a height of 1 m. A library of roofs, pavements, park grass, farm crops, and other materials covering the major land cover features over the study area was built. Besides, pixel purity index was combined with N-dimensional visualizer to select some candidate image endmembers. This process would radically improve the accuracy of spectrum extraction since some large-scale features
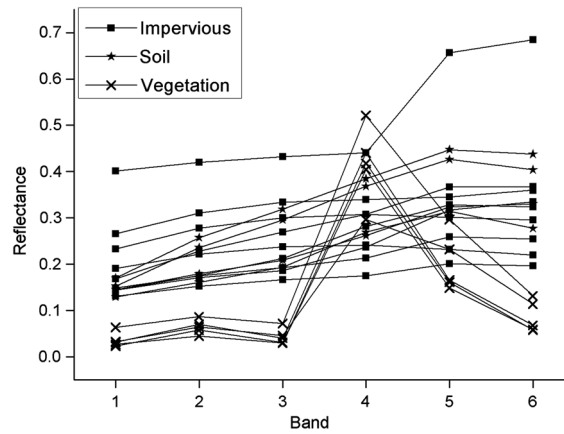
Fig. 3 Spectral reflectance of endmembers used for the multiple endmember spectral mixture analysis.

cannot be captured by field campaign. Finally, ENVI-add on Viper Tools (www.vipertools.org) was utilized to identify a diversity of spectra most representing each category following the VIS model, and the collected reflectance spectra are shown in Fig. 3.

Using the spectrum library composed of field spectra and image spectra, spectral unmixing is performed by selecting all the combinations of endmembers iteratively. A total of 18 representative nonshade endmembers were collected. The impervious surface category included nine distinct endmembers spectra, while the vegetation and bare soil included five and four spectra, respectively. Consequently, a total of 299 combination models were employed to characterize each pixel, 18 of which were one-model, 101 two-model, and 180 three-model. Several model constraints were imposed on maximum RMSE and maximum allowable shade fraction. The model satisfying all the constraints and having the lowest RMSE was chosen to estimate category fractions for each pixel. The result of MESMA was an image with 19 bands representing the fractions of impervious surface, vegetation, soil, and shade, respectively. Since shade endmember is a variable spectra that we would not be interested in, the normalization was performed through dividing each endmember fraction by the total of nonshade fractions. These normalized bands were used to not only calculate urban impervious surface fractions, but also estimate surface spectral emissivity later.

3.3 Methodology of LST Retrieval

LST was retrieved from geometrically corrected Landsat TM 6 band (10.44 to 12.42 μm). First, the digital number of Landsat thermal band was converted to spectral radiance, and then converted to at-satellite brightness temperature as follows:

$$L = 0.0056322 * \text{DN} + 0.1238, \tag{1}$$

$$T_b = \frac{K_2}{\ln[(K_1/L) + 1]}, \tag{2}$$

where T_b is the brightness temperature in Kelvin, L is spectral radiance, and K_1 and K_2 are the calibration constants in mWcm^{-2} sr^{-1} μm^{-1} ($K_1 = 60.776$ and $K_2 = 1260.5$). Last, surface temperature could be estimated as

$$\text{LST} = \frac{T_b}{1 + (\lambda * T_b/\rho) \ln \varepsilon}, \tag{3}$$

$$\rho = \frac{h * c}{\sigma}, \tag{4}$$

where λ is the wavelength of emitted radiance ($\lambda = 11.5$ μm), σ is the Boltzmann constant (1.38×10^{-23} J/K), h is the Planck's constant (6.626×10^{-34} Js), and c is the velocity of light (2.998×10^{8} m/s).

Spectral emissivity is a key parameter that directly influences the accuracy of LST retrieval. Various approaches have been developed to obtain spectral emissivity for a heterogeneous and nonisothermal pixel, and one of the most common methods is spectral mixture analysis, which mainly involves visible and near-infrared bands. Here, the fraction images of MESMA were incorporated with representative broadband spectral emissivity to retrieve pixel-level surface emissivity. The broadband spectral emissivity of typical land cover types were derived from field experiment and spectral libraries, and its associated information is shown in Table 2. The spectral emissivity value of each pixel could be derived as

$$\varepsilon = \sum_{k=1}^{n} \varepsilon_k . f_k,$$

(5)

where ε is the spectral emissivity corresponding to endmember k and f_k is the fraction of endmember k within the pixel. Since the constraints imposed on MESMA were slightly strict, there existed some pixels unmolded by candidate models. For these pixels, NDVI thresholds method[27] was adopted to calculate pixel-level emissivity. NDVI^{THM} is a semiempirical method in which spectral emissivity is obtained from vegetation fraction in consideration of different landscapes.

3.4 Temperature Emissivity Separation Algorithm

Temperature emissivity separation (TES)[28] algorithm was adopted to retrieve high-resolution LST for TASI airborne hyperspectral thermal image. TES mainly consists of three modules: normalized emissivity method (NEM), ratio, and maximum-minimum difference (MMD). NEM is performed to obtain surface radiometric temperature, and ratio algorithm is used to obtain emissivity ratios. The β spectral shape of emissivity, which is obtained using ratios of each channel emissivity to their mean value, is also applied to reduce instrumental noise. TES generally utilizes the relationship among minimum emissivity value $\varepsilon_{\min}$ and the variations of emissivity spectral to characterize magnitude, the form of which is MMD in this analysis:

$$\mathrm{MMD} = \varepsilon_{\max} - \varepsilon_{\min}.$$

(6)

A semi-empirical relationship between $\varepsilon_{\min}$ and MMD was established by Yang et al.,[29] and the result of statistical fitting could be modified as

$$\varepsilon_{\min} = 0.992 - 0.917 * \mathrm{MMD}^{0.972}.$$

(7)

Table 2 Spectral emissivity used to derive land surface temperature (LST).

Type	Emissivity	Derivation description
Concrete pavement	0.9047	Field collected
Asphalt pavement	0.906	Field collected
Granite pavement	0.9044	Field collected
Roof	0.82785	Field collected
Soil	0.9593	Field collected/Aster spectral library
Grass	0.9809	Field collected
Crop	0.983	Field collected/Aster spectral library

4 Results and Discussion

4.1 *Land Surface Imperviousness*

The fraction images of MESMA can describe the spatial distribution of individual land cover component, and the results are shown in Fig. 4. Pixel values of each estimated image represent the areal proportions of associated endmember within a pixel. The ISA map was obtained by summing over all the endmember fractions belonging to impervious surface. It is observed that the values were within the range of −0.02 to 1.05, with a mean value of 0.317 and standard deviation (SD) of 0.22. Higher fraction covers of impervious surface were recorded in the part of central, northern, and southwestern areas of the image. These areas were corresponding to urban and high-dense suburb area. Contrarily, the lower fraction covers were distributed in the eastern and northwestern region, which were corresponding to low-dense suburb area and bare soil. Over the impervious fraction image, it appeared that the values were becoming lower from the center to margin, meaning that impervious surface was mainly located in the center urban area.

For the vegetation fraction image obtained by summing over all the vegetation endmember fractions, park grassland and crop contained higher values, while impervious surface and bare soils had lower values. The vegetation fractions were somewhat consistently lower than the values of NDVI. This is most likely due to the fact that the phenology of farm crop over Shijiazhuang city was put off as a consequence of a super snow disaster. In the soil fraction image, soil was observed with higher values, while crop and suburb areas had the opposite form as well as impervious surface. Overall, the fraction images have exhibited spatial patterns with high visual accuracy.

To better understand LST spatial distribution, the study area was divided into five classes: water, vegetation, soil, and urban area in low and high density. Two land covers within the impervious surface were reclassified in consideration of urban area density. The first class is mostly commercial land with a high density, while the second class is residential land and transportation with a low density. An empirical value of 0.6 was accessed to distinguish these two different urban impervious covers. The imperviousness pixels were assigned to high-dense urban unless their percentage ISA values were >60%. The result of subpixel classification is shown in Fig. 4(d).
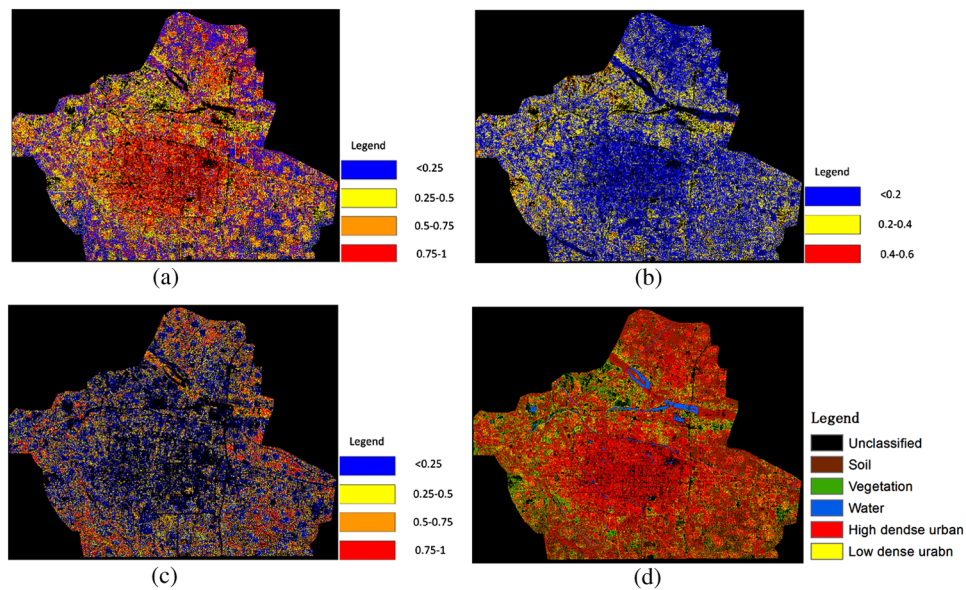

Fig. 4 Fraction images and land cover map derived from LANDSAT TM imagery using multiple endmember spectral mixture analysis. (a) Impervious surface fractions. (b) Vegetation fractions. (c) Soil fractions. (d) Land cover map.
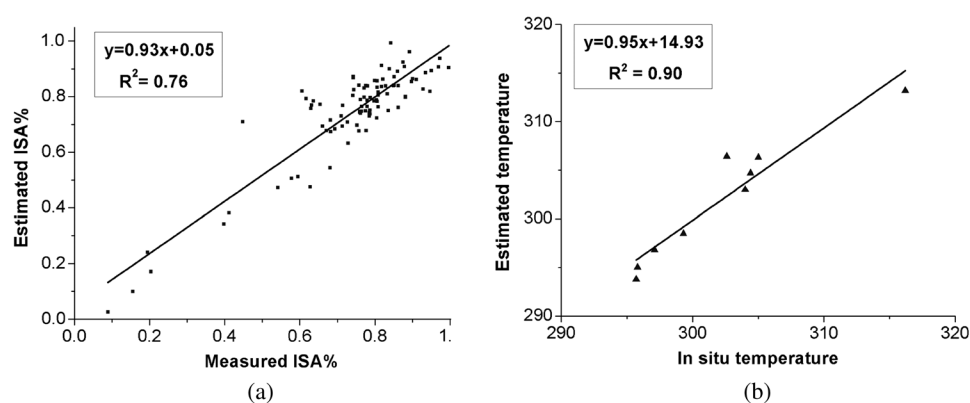
Fig. 5 Accuracy assessment results of (a) estimated impervious surface from the Landsat TM image and (b) estimated surface temperature from the thermal airborne spectrographic imager (TASI) image.

Concerning the quality of impervious image retrieved from MESMA, sufficient reference data were selected to perform precision evaluation. A total of 90 sample plots were identified on the impervious surface image through a suitable sampling scheme, and the corresponding actual ISA values were obtained from WV2 image with a high spatial resolution of 0.5 m. Figure 5 reveals that the estimated result presents a satisfactory accuracy with a coefficient of determination R^2 of 0.76. As suggested by Yang et al.,[30] if a sufficient number of spectra could be collected to adequately represent the spectral variation of the material on the ground, the MESMA method promises to give an accurate ISA estimation. In this research, a diversity of field spectra was collected to perform spectral mixing analyses in the hope to reveal the potential of MESMA for retrieving ISA. Furthermore, it is noted that MESMA method indeed improves the ISA estimation accuracy through varying the number and type of endmembers, especially in the medium- and high-ISA areas. However, the samples of low percentage ISA (<0.6) tended to be underestimated due to the mixture of soil and shade. Overall, MESMA approach is proved effective in extracting impervious surfaces, and its estimated results are suitable for further qualitative analysis.

4.2 *LST, Impervious Surface Area, and NDVI*

LST was retrieved through a method that considers pixel-level spectral emissivity as a linear combination of the representative emissivity. The estimated image and statistics of LST are shown in Fig. 6(a) and Table 3. It is observed that the surface temperature ranged from
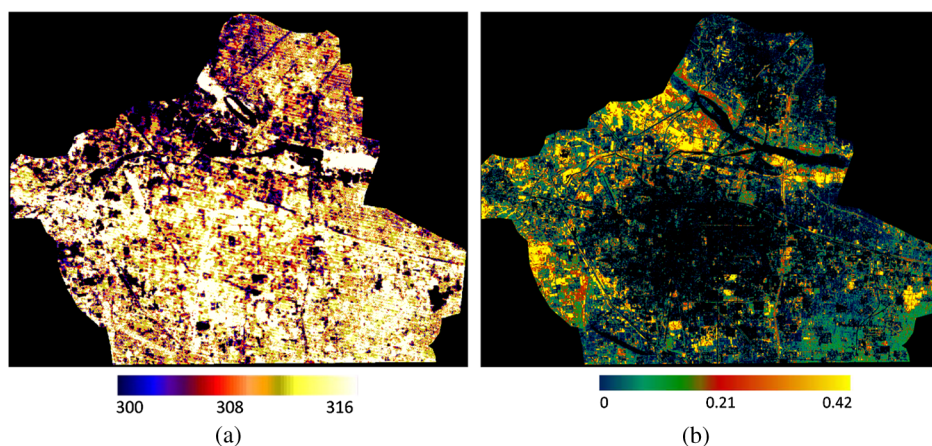

Fig. 6 (a) Land surface temperature (LST) image retrieved from LANDSAT thermal image with our method. (b) Normalized difference vegetation index (NDVI) image.

Table 3 Descriptive statistics for LST over different land cover types in LANDSAT TM imagery.

Land cover class	Min	Max	Mean	Stddev	Area in %
Soil	28.5184	40.989	34.5246	1.17506	29.6
Vegetation	27.3861	39.1268	33.1331	1.60758	9.8
High-density urban	28.87	41.5335	34.7556	2.06737	46.5
Low-density urban	28.2781	41.1352	33.9046	1.43016	12

26.87 to 41.53°C, with a mean value of 34.24°C. The central and eastern parts of LST imager exhibited maximum surface temperature. These areas were corresponding to ISAs. It is also observed that some parts of northern-western mainly occupied by crop and grass had lower surface temperature. The spatial pattern of LST over Shijiazhuang city reveals that the city center exhibits the highest temperature, and the temperature tends to decrease from the urban center to the surrounding rural areas. Many studies in the literature relevant to UHI have proved that LST is closely associated with land cover; therefore, it was meaningful to explore the relationship among them to help understand UHI.[31,32] Specifically, vegetation had the lowest temperature ranging from 27.39 to 39.13°C, with a mean value of 33.13°C and SD of 1.61°C. The smaller temperature variation of vegetation results from its thermal capacities, which make it easy to reduce heat stored through transpiration. Surface temperature of bare soil was between 28.52 and 40.99°C, having a mean value of 34.52 °C and SD of 1.18°C. Influenced by factors such as evapotranspiration, humidity content, and surrounding ecosystem, desert soil distributed in north China generally has little ability to store absorbed energy. Consequently, a thermal response similar to that of urban impervious surface occurred for desert soil over the study area. It is noted that the average LST of high-dense urban was higher than that of low-dense urban. The surface temperature of the high-dense urban area ranged from 28.87 to 41.53°C, with a mean temperature of 34.76°C and SD of 2.07°C, while for the low-dense urban land, surface temperature ranged from 28.28 to 41.14°C, with a mean value of 33.90° C and SD of 1.43°C. This can be partly contributed to the high-dense population and human activities of high-dense urban surfaces. Moreover, the maximum SD of LST was still recorded in high-dense urban area among all the urban covers, implying these regions had experienced a large variation in temperature mainly caused by the heterogeneity of impervious materials.

For the NDVI image displayed in Fig. 6(b), bright areas indicate dense vegetation, while the dark areas indicate sparse ones. An inverse model of NDVI was exhibited in LST map, probably due to the capacity of urban canopy in mitigating the amount of heat store. It is well known that the analysis concerning LST and NDVI can provide more detailed information about urban conditions. Moreover, a scatterplot of LST and NDVI is usually expressed by the triangular form resembling the results shown in Fig. 7(a). The upper and bottom edge of triangle scatter gram of NDVI-LST are termed as warm edge and cool edge, respectively,[33] both of which are significant for studying surface energy balance.[34] The warm edge is observed to have a negative slope, indicating the cooling effect of vegetation, and this is primarily due to the demand of high surface energy for vegetation transpiration. Various previous studes have revealed a strong linear relationship between LST and ISA.[18,21,35] However, Fig. 7(c) shows that there was no significant relationship between LST and percent ISA in Shijiazhuang city. The reason is that the heterogeneity of urban material makes impervious surfaces easily confused with bare soil and fallow land, especially with respect to the areas where percentage ISA was <50%. Besides, a higher LST may occur for bare soil rather than bright urban surface, therefore leading to a more complex urban condition.

To further investigate the correlations among LST, NDVI, and ISA, a quantitative analysis was carried out to evaluate the average LST at the increment of the NDVI from 0.1 to 1, and at the increment of percentage ISA from 0 to 100%. Regarding regional mean values, a weaker but significant linear relationship was displayed among LST, percent imperviousness, and NDVI as shown in Figs. 7(b) to 7(d). It is interesting to note that the linear relations among them were
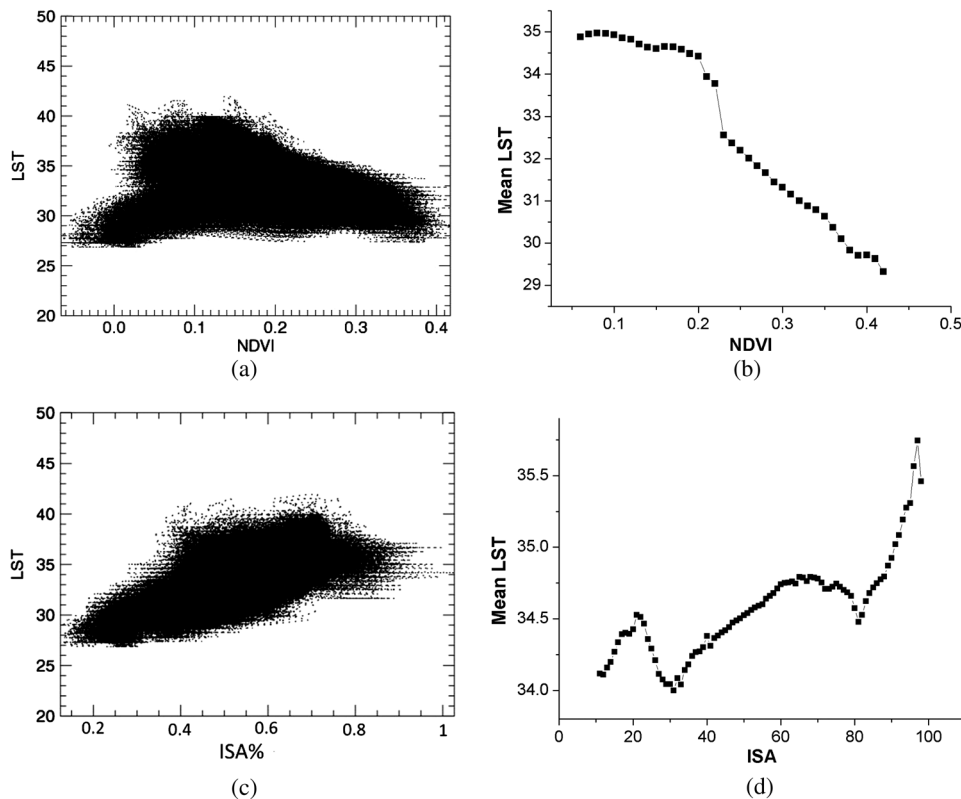
Fig. 7 Scatterplots of (a) LST versus NDVI, (b) mean LST versus NDVI, (c) LST versus percent impervious surface area (ISA), and (d) mean LST versus ISA.

slightly evident over the whole range because of the confusion between vegetation and impervious surfaces. However, when it came to a certain value, a stronger linear relationship appeared in LST-NDVI (>0.1) as well as in LST-ISA (>30).

4.3 *LST Derived from TASI Imagery*

For the purpose of investigating the spatial distribution of urban thermal patterns at local levels, the LST map covering part of the Shijiazhuang city center was designed using the TASI image. The algorithm used was ASTER TES and the retrieval result is shown in Fig. 8(a). In total, nine targets were selected to make comparison between TASI measurements and concurrent ground temperatures. This involves three natural surfaces (green grass and crop), five manmade surfaces (two distinct roofs and three distinct pavements), and water body. TASI measurements were extracted from the LST map with 3×3 pixel windows, while *in situ* values were acquired from the average concurrent ground temperature measured. Figure 5(b) shows a strong agreement between TASI-derived temperatures and *in situ* values, with a mean absolute difference of 1.47 and an RMSE of 0.62.

Relating LST to distinct land cover features through high-resolution airborne thermal sensor can help us further grasp the establishment of UHI. To study the influence of land covers on the variations of LST, a high-precision classification map was designed using WV2 image and SASI image, the spatial resolutions of which are 2 and 1.25 m, respectively. Spectral-spatial classification was adopted to divide the whole image into five ground-truth classes: water, soil, vegetation, metal rooftops, and built-up areas. This approach is based on the fusion of the watershed segmentation with support vector machine classifier.[36] Concerning surface temperature of distinct land-cover composition, the maximum mean LST was recorded in metal rooftops, followed by built-up areas containing pavements and buildings. The three other covers had a lower average LST compared to impervious areas. It should be noted that the collected date of airborne thermal imagery was just during summer when Shijiazhuang has experienced
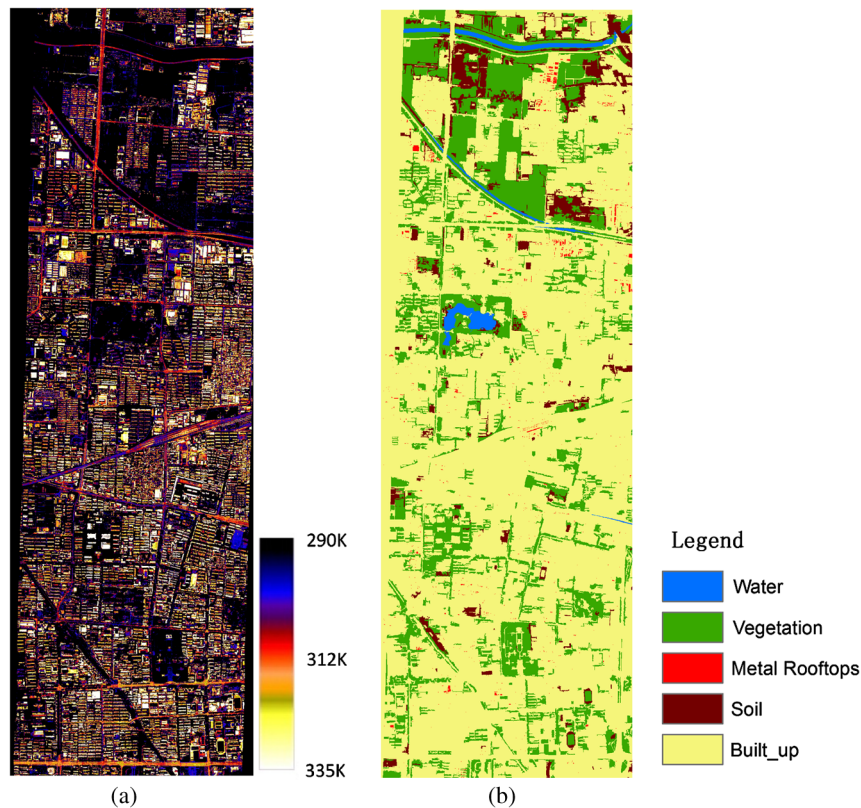
Fig. 8 (a) LST image retrieved from TASI image with temperature emissivity separation method. (b) Land cover map produced from WorldView-2 imagery using support vector machine and watershed segmentation method.

the highest temperature. The rooftop had a mean LST of 44.61℃ and an SD of 6.19℃, while built-up areas had a lower average value of 38.48℃ and an SD of 6.29℃. The SD value of LST was generally larger for urban areas than the vegetation areas, indicating that the impervious surfaces would have experienced a wider variation in LST because of different building structures and construction materials. This further explains the thermal heterogeneity over urban areas. Water area mostly located in river and park had the lowest mean average LST of 32.22℃. The statistical values and a frequency histogram over different land cover types are shown in Table 4 and Fig. 9. From the results of Fig. 9, it is observed that both metal rooftops and built-up areas have a higher variability and wider extent in temperature as a consequence of the heterogeneity of imperviousness surfaces, which is easily affected by many factors, such as thermal properties and anthropogenic activity. Additionally, a revised mean UHI intensity was computed as the difference between mean temperatures of the impervious surface and the pervious cover (UHI $= T_{\text{mean-impervious}} - T_{\text{mean-pervious}}$).[8,13] For the TASI thermal imagery,

Table 4 Descriptive statistics for LST over different land cover types in TASI imagery.

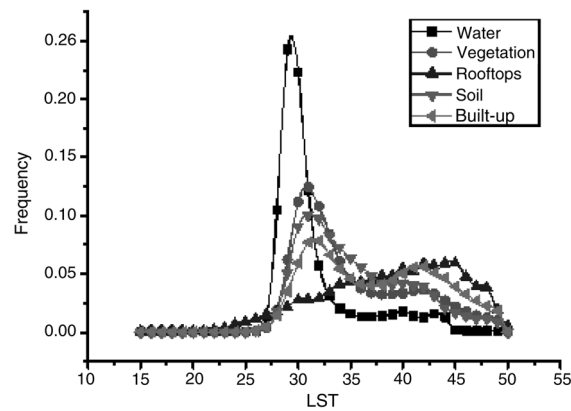| Land cover class	Mean	Stddev	Description
Water	32.2198	4.2407	Rivers, lakes
Vegetation	36.1256	5.94574	Farmland, gardens
Rooftops	44.6055	6.1896	Metal rooftops of factories and marketplace
Soil	36.3621	5.63521	Bare soil, fallow
Built-up	38.4775	6.28086	Roads, buildings, residential areas

Fig. 9 Histogram shows the frequency distribution over all land cover.

the August 15, 2010, scene shows a mean UHI intensity of 2.52°C in Shijiazhuang. The result is similar to that of Landsat data, revealing that an urban heat island is evident in Shijiazhuang and impervious surface is contributing most to this phenomenon.

5 Conclusion

This paper demonstrated how NDVI and surface fraction images can be employed to relate urban surface thermal patterns to land cover features in the case of Shijiazhuang, China. At the regional level, LST was positively correlated with impervious surface, while it represented a negative correlation with vegetation area. This suggests that an increasing proportion of impervious surface would lead to heat island effects, and thus, special attention should be paid. In addition, MESMA approach was utilized to retrieve accurate LST and ISA through taking advantage of the visible and near-infrared bands of Landsat TM imagery.

In this study, qualitative and quantitative analysis was conducted to examine the relationships between LST and other surface parameters through the two thermal sensors. Landsat TM image with a thermal band of 120-m resolution allows delineation of relatively coarse thermal patterns. While considering the high heterogeneity of urban environments, airborne thermal sensor is more desirable since it can provide high spatial resolution and spectral resolution. Overall, results indicate that different spatial scales are requested in urban thermal characteristic studies.

With the aid of MESMA, an overall emissivity for given pixel can be retrieved by combining the fraction of each cover component with respective emissivity values. Although rare studies use MESMA technique to estimate surface emissivity, SMA has proven to be efficient in describing urban thermal characteristics. Therefore, our results complement the findings of a small number of previous studies[37,38] that support the use of SMA in calculating surface emissivity due to its strong capacity in retrieving fractions representative of subpixel components. However, optical bands of Landsat TM imagery may not be suitable for performing SMA well because of its limited spectral resolution. The hyperspectral imagery providing detailed spectral data for information extraction, therefore, should have the great potential in obtaining overall pixel-level emissivity, and more concern will be put into this in further studies.

Acknowledgments

References

1. Q. Weng, "Thermal infrared remote sensing for urban climate and environmental studies: methods, applications, and trends," *ISPRS J. Photogramm. Remote Sens.* **64**(4), 335–344 (2009), http://dx.doi.org/10.1016/j.isprsjprs.2009.03.007.

2. J. A. Voogt and T. R. Oke, "Thermal remote sensing of urban climates," *Remote Sens. Environ.* **86**(3), 370–384 (2003), http://dx.doi.org/10.1016/S0034-4257(03)00079-8.

3. I. Keramitsoglou et al., "Identification and analysis of urban surface temperature patterns in Greater Athens, Greece, using MODIS imagery," *Remote Sens. Environ.* **115**(12), 3080–3090 (2011), http://dx.doi.org/10.1016/j.rse.2011.06.014.

4. N. Schwarz, S. Lautenbach, and R. Seppelt, "Exploring indicators for quantifying surface urban heat islands of European cities with MODIS land surface temperatures," *Remote Sens. Environ.* **115**(12), 3175–3186 (2011), http://dx.doi.org/10.1016/j.rse.2011.07.003.

5. M. Stathopoulou, C. Cartalis, and I. Keramitsoglou, "Mapping micro-urban heat islands using NOAA/AVHRR images and CORINE land cover: an application to coastal cities of Greece," *Int. J. Remote Sens.* **25**(12), 2301–2316 (2004), http://dx.doi.org/10.1080/01431160310001618725.

6. U. Rajasekar and Q. Weng, "Urban heat island monitoring and analysis using a non-parametric model: a case study of Indianapolis," *ISPRS J. Photogramm. Remote Sens.* **64**(1), 86–96 (2009), http://dx.doi.org/10.1016/j.isprsjprs.2008.05.002.

7. G. Xian and M. Crane, "An analysis of urban thermal characteristics and associated land cover in Tampa Bay and Las Vegas using Landsat satellite data," *Remote Sens. Environ.* **104**(2), 147–156 (2006), http://dx.doi.org/10.1016/j.rse.2005.09.023.

8. M. Tiangco, A. M. F. Lagmay, and J. Argete, "ASTER-based study of the night-time urban heat island effect in Metro Manila," *Int. J. Remote Sens.* **29**(10), 2799–2818 (2008), http://dx.doi.org/10.1080/01431160701408360.

9. G. Cai, M. Du, and Y. Xue, "Monitoring of urban heat island effect in Beijing combining ASTER and TM data," *Int. J. Remote Sens.* **32**(5), 1213–1232 (2011), http://dx.doi.org/10.1080/01431160903469079.

10. R. Pu et al., "Assessment of multi-resolution and multi-sensor data for urban surface temperature retrieval," *Remote Sens. Environ.* **104**(2), 211–225 (2006), http://dx.doi.org/10.1016/j.rse.2005.09.022.

11. R. Oltra-Carrió et al., "Land surface emissivity retrieval from airborne sensor over urban areas," *Remote Sens. Environ.* **123**, 298–305 (2012), http://dx.doi.org/10.1016/j.rse.2012.03.007.

12. R. Gluch, D. A. Quattrochi, and J. C. Luvall, "A multi-scale approach to urban thermal analysis," *Remote Sens. Environ.* **104**(2), 123–132 (2006), http://dx.doi.org/10.1016/j.rse.2006.01.025.

13. J. A. Sobrino et al., "Evaluation of the surface urban heat island effect in the city of Madrid by thermal remote sensing," *Int. J. Remote Sens.* **34**(9–10), 3177–3192 (2013), http://dx.doi.org/10.1080/01431161.2012.716548.

14. Y. Zhang, I. O. A. Odeh, and C. Han, "Bi-temporal characterization of land surface temperature in relation to impervious surface area, NDVI and NDBI, using a sub-pixel image analysis," *Int. J. Appl. Earth Obs. Geoinf.* **11**(4), 256–264 (2009), http://dx.doi.org/10.1016/j.jag.2009.03.001.

15. Q. Weng, D. Lu, and J. Schubring, "Estimation of land surface temperature–vegetation abundance relationship for urban heat island studies," *Remote Sens. Environ.* **89**(4), 467–483 (2004), http://dx.doi.org/10.1016/j.rse.2003.11.005.

16. X. Zhang et al., "Estimation of the relationship between vegetation patches and urban land surface temperature with remote sensing," *Int. J. Remote Sens.* **30**(8), 2105–2118 (2009), http://dx.doi.org/10.1080/01431160802549252.

17. Q. Weng, "Remote sensing of impervious surfaces in the urban areas: requirements, methods, and trends," *Remote Sens. Environ.* **117**, 34–49 (2012), http://dx.doi.org/10.1016/j.rse.2011.02.030.

18. F. Yuan and M. E. Bauer, "Comparison of impervious surface area and normalized difference vegetation index as indicators of surface urban heat island effects in Landsat imagery,"

Remote Sens. Environ. **106**(3), 375–386 (2007), http://dx.doi.org/10.1016/j.rse.2006.09.003.

19. J. Li et al., "Impacts of landscape structure on surface urban heat islands: a case study of Shanghai, China," *Remote Sens. Environ.* **115**(12), 3249–3263 (2011), http://dx.doi.org/10.1016/j.rse.2011.07.008.

20. J. Mallick, A. Rahman, and C. K. Singh, "Modeling urban heat islands in heterogeneous land surface and its correlation with impervious surface area by using night-time ASTER satellite data in highly urbanizing city, Delhi-India," *Adv. Space Res.* **52**(4), 639–655 (2013), http://dx.doi.org/10.1016/j.asr.2013.04.025.

21. D. Lu and Q. Weng, "Spectral mixture analysis of ASTER images for examining the relationship between urban thermal features and biophysical descriptors in Indianapolis, Indiana, USA," *Remote Sens. Environ.* **104**(2), 157–167 (2006), http://dx.doi.org/10.1016/j.rse.2005.11.015.

22. Q. Weng and D. Lu, "A sub-pixel analysis of urbanization effect on land surface temperature and its interplay with impervious surface and vegetation coverage in Indianapolis, United States," *Int. J. Appl. Earth Obs. Geoinf.* **10**(1), 68–83 (2008), http://dx.doi.org/10.1016/j.jag.2007.05.002.

23. T. H. Painter et al., "The effect of grain size on spectral mixture analysis of snow-covered area from AVIRIS data," *Remote Sens. Environ.* **65**(3), 320–332 (1998), http://dx.doi.org/10.1016/S0034-4257(98)00041-8.

24. D. A. Roberts et al., "Optimum strategies for mapping vegetation using multiple-endmember spectral mixture models," *Proc. SPIE* **3118**, 108–119 (1997), http://dx.doi.org/10.1117/12.278930.

25. C. Quintano, A. Fernández-Manso, and D. A. Roberts, "Multiple endmember spectral mixture analysis (MESMA) to map burn severity levels from Landsat images in Mediterranean countries," *Remote Sens. Environ.* **136**, 76–88 (2013), http://dx.doi.org/10.1016/j.rse.2013.04.017.

26. G. L. Feyisa et al., "Automated water extraction index: a new technique for surface water mapping using Landsat imagery," *Remote Sens. Environ.* **140**, 23–35 (2014), http://dx.doi.org/10.1016/j.rse.2013.08.029.

27. J. Sobrino, N. Raissouni, and Z.-L. Li, "A comparative study of land surface emissivity retrieval from NOAA data," *Remote Sens. Environ.* **75**(2), 256–266 (2001), http://dx.doi.org/10.1016/S0034-4257(00)00171-1.

28. A. Gillespie et al., "A temperature and emissivity separation algorithm for advanced spaceborne thermal emission and reflection radiometer (ASTER) images," *IEEE Trans. Geosci. Remote Sens.* **36**(4), 1113–1126 (1998), http://dx.doi.org/10.1109/36.700995.

29. H. Yang et al., "Algorithm of emissivity spectrum and temperature separation based on TASI data," *J. Remote Sens.* **15**(6), 1242–1254 (2011), http://dx.doi.org/10.11834/jrs.20110380.

30. F. Yang, B. Matsushita, and T. Fukushima, "A pre-screened and normalized multiple endmember spectral mixture analysis for mapping impervious surface area in Lake Kasumigaura Basin, Japan," *ISPRS J. Photogramm. Remote Sens.* **65**(5), 479–490 (2010), http://dx.doi.org/10.1016/j.isprsjprs.2010.06.004.

31. I. J. A. Callejas et al., "Relationship between land use/cover and surface temperatures in the urban agglomeration of Cuiabá-Várzea Grande, Central Brazil," *J. Appl. Remote Sens.* **5**(1), 053569 (2011), http://dx.doi.org/10.1117/1.3666044.

32. X.-L. Chen et al., "Remote sensing image-based analysis of the relationship between urban heat island and land use/cover changes," *Remote Sens. Environ.* **104**(2), 133–146 (2006), http://dx.doi.org/10.1016/j.rse.2005.11.016.

33. Z. Gao, W. Gao, and N.-B. Chang, "Integrating temperature vegetation dryness index (TVDI) and regional water stress index (RWSI) for drought assessment with the aid of LANDSAT TM/ETM+ images," *Int. J. Appl. Earth Obs. Geoinf.* **13**(3), 495–503 (2011), http://dx.doi.org/10.1016/j.jag.2010.10.005.

34. L. Jiang and S. Islam, "A methodology for estimation of surface evapotranspiration over large areas using remote sensing observations," *Geophys. Res. Lett.* **26**(17), 2773–2776 (1999), http://dx.doi.org/10.1029/1999GL006049.

35. E. Dumas, M. Jappiot, and T. Tatoni, "Mediterranean urban-forest interface classification (MUFIC): a quantitative method combining SPOT5 imagery and landscape ecology indices," *Landsc. Urban Plan.* **84**(3–4), 183–190 (2008), http://dx.doi.org/10.1016/j.landurbplan.2007.12.002.

36. L. Shafarenko, M. Petrou, and J. Kittler, "Automatic watershed segmentation of randomly textured color images," *IEEE Trans. Image Process.* **6**(11), 1530–1544 (1997), http://dx.doi.org/10.1109/83.641413.

37. B. Feizizadeh and T. Blaschke, "Examining urban heat island relations to land use and air pollution: multiple endmember spectral mixture analysis for thermal remote sensing," *IEEE J. Sel. Topics Appl. Earth Obs. Remote Sens.* **6**(3), 1749–1756 (2013), http://dx.doi.org/10.1109/JSTARS.2013.2263425.

38. Z. Mitraka et al., "Improving the estimation of urban surface emissivity based on sub-pixel classification of high resolution satellite imagery," *Remote Sens. Environ.* **117**, 125–134 (2012), http://dx.doi.org/10.1016/j.rse.2011.06.025.

Kai Liu received his MS degree in electronic and communication engineering from the Institute of Remote Sensing and Digital Earth, Beijing City, China, in 2013. He is currently pursuing his PhD degree in cartography and geographical information systems. His research focuses on the application of thermal infrared and hydrological remote sensing methods to the study of land use and anthropogenic activities, urban heat islands, and surface energy and water balance.

Biographies of the other authors are not available.